ISSN 1027-4510, Journal of Surface Investigation: X-ray, Synchrotron and Neutron Techniques, 2019, Vol. 13, No. 6, pp. 995–1004. © Pleiades Publishing, Ltd., 2019.
Russian Text © The Author(s), 2019, published in Poverkhnost', 2019, No. 11, pp. 3–13.

Comprehensive Investigation of Some Ordinary Chondrites Based on X-Ray Methods and Mössbauer Spectroscopy

L. V. Guda[a], A. N. Kravtsova[a, *], A. A. Guda[a], S. P. Kubrin[b], M. I. Mazuritskiy[c], and A. V. Soldatov[a]

[a] *Smart Materials Research Institute, Southern Federal University, Rostov-on-Don, 344090 Russia*
[b] *Research Institute of Physics, Southern Federal University, Rostov-on-Don, 344090 Russia*
[c] *Physics Faculty, Southern Federal University, Rostov-on-Don, 344090 Russia*
**e-mail: akravtsova@sfedu.ru*

Received December 28, 2018; revised February 19, 2019; accepted February 19, 2019

Abstract—Comprehensive investigation into ordinary chondrites presented by the species of Markovka (H4 petrological type), Polujamki (H4 type) and Jiddat Al Harasis 055 (L4-5 type) is performed. The element and phase compositions, as well as the oxidation states of iron and nickel in the chondrites, are examined via micro X-ray fluorescence (micro-XRF), Mössbauer spectroscopy and synchrotron-based X-ray absorption spectroscopy. Elemental composition analysis is performed using micro-XRF, allowing one to obtain element distribution maps for the meteorite samples. According to Mössbauer spectroscopy data gathered on iron-containing phases, the chondrites consist mainly of olivine and goethite with a small amount of pyroxene and hematite. A low amount of troilite and kamacite is also observed in the Markovka and Polujamki specimens. The oxidation states of 3d metals in the chondrites are estimated from Fe and Ni *K*-edge X-ray absorption near-edge structure (XANES) spectra. Most nickel atoms in the meteorites are found to be in the Ni^{2+} state, while iron has an average oxidation state of +2.4 which is commensurate with the Mössbauer spectroscopy data. Infrared spectroscopy analysis of the chondrites is implemented as well. The results are important from the viewpoint of statistics acquisition on ordinary chondrites, as well as for further understanding of their formation.

Keywords: meteorites, ordinary chondrites, element and phase composition, iron and nickel oxidation state, micro XRF analysis, element mapping, Mössbauer spectroscopy, X-ray absorption spectroscopy, XANES

DOI: 10.1134/S1027451019060089

INTRODUCTION

Meteorites are the main source of information on the earlier stages of solar-system evolution. Most meteorites are ordinary chondrites. Although meteorites have been comprehensively studied, complex investigations into their element and phase distributions, especially at the microscale level, have not been performed to date.

A nondestructive spectral technique that is typically used for the elemental composition analysis of meteorites is X-ray fluorescence (XRF) [1]. According to [2], there is a database XRF spectra devoted to meteorites. Since meteorites are inhomogeneous, particular attention is also paid to plotting the element distribution map [3] via micro-X-ray fluorescence (micro-XRF) [4]. Mössbauer spectroscopy is another well-known method for studying ordinary chondrites [5–9]. It is used in the detection of iron-containing phases in meteorites, as well as in the evaluation of iron oxidation states. Infrared (IR) spectroscopy is less applied for the investigation of meteorites [10–14]. This technique enables one to study insoluble organic substances extracted from meteorites [10, 11], as well as to monitor any changes within the meteorite structure caused by impact effects [12, 13].

In recent years, investigations based on the X-ray absorption spectroscopy (XAS) of meteorite matter have become of increasing interest [15, 16]. Since XAS belongs to the group of local, element-selective characterization tools, it supplements unique methods for probing the atomic and electronic structure and can therefore be used in the study of materials free of long-range order in the arrangement of atoms, including amorphous sites in meteorites.

The fine structure of the X-ray absorption spectrum is formed by the X-ray absorption near-edge structure (XANES) and the extended X-ray absorption near-edge structure (EXAFS). EXAFS spectroscopy enables one to determine the coordinate numbers and interatomic distances around the selected absorbing type of atoms. While XANES spectroscopy [17] ensures highly accurate information on the three-dimensional atomic structure around the absorbing type of atoms (e.g. bond lengths and bond angles) and allows one to analyze the peculiarities of an electronic

subsystem, i.e., to evaluate the oxidation state of 3*d*-metals in meteorites via chemical-shift analysis of EXAFS and XANES spectra.

XAS has recently been applied in investigations of the atomic and electronic structure of geological materials [18–24]. Meanwhile, X-ray spectroscopy is still poorly used in cosmogeochemistry because of difficulties in data interpretation and the poor availability of unique experimental facilities (third-generation synchrotronic centers). Many works are dedicated to the analysis of C and N *K*-edges XANES spectra of meteorites [25–28], less often Fe *K*-edge XANES [29–34]. The most studied by XANES spectroscopy are carbonaceous chondrites [34, 35]. Despite making up the majority of meteorites, ordinary chondrites are still poorly understood [36, 37], especially by X-ray spectral techniques [38].

The present work is aimed at the comprehensive investigation of a series of ordinary chondrites, such as Markovka, Polujamki and Jiddat Al Harasis 055.

The Markovka chondrite (H4 petrological type) was discovered in 1967 near the Markovka village (Russian Federation, 52°24′ N, 79°48′ E) [39]. The Polujamki chondrite (H4 type) was found close to Mikhailovskoe village (Russian Federation, 52°6′ N, 79°42′ E). The Jiddat Al Harasis 055 chondrite (L4–L5 petrological type) was discovered in Oman (19°39.31′ N, 56°41.758′ E) in 2004 [41]. Comprehensive diagnostics of the Markovka, Polujamki and Jiddat Al Harasis 055 chondrites includes element analysis and mapping at the microscale level, the detection of iron-containing phases and the analysis of XANES spectra with estimation of the oxidation state of 3*d*-metals (iron and nickel). The micro-XRF method is used for the determination and micromapping of the elemental composition in specimens. The analysis of iron-containing phases of the chondrites is implemented via Mössbauer spectroscopy. The oxidation state of iron in the meteorites is determined from combined analysis of the Mössbauer spectra and Fe *K*-edge XANES spectra. The oxidation state of nickel is estimated from the Ni *K*-XANES spectra. In addition to X-ray techniques and Mössbauer spectroscopy, the chondrites are also probed via IR spectroscopy. Comprehensive diagnostics of the Markovka, Polujamki and Jiddat Al Harasis 055 meteorites is essential from the viewpoint of data acquisition on the chemical composition and structure of ordinary chondrites. Statistical data acquisition on various meteorites, as well as their characterization at the microlevel, is an actual task, which is fundamental for the correct description of processes during the formation of a protoplanetary disk, including the coagulation and differentiation of interstellar matter in the early Solar System.

EXPERIMENTAL

Meteorite samples are known for their inhomogeneous structure, hence elemental composition analysis and element distribution mapping in the chondrites was performed via micro-XRF using an M4 TORNADO (Bruker) microfluorescence spectrometer with a spatial resolution of 25 μm. The operation conditions of the X-ray tube were as follows: $U = 50$ kV and $I = 600$ μA. The working vacuum of the chamber (20 mbar) allows one to perform the micro-XRF measurements of chemical elements starting from Na. The chondrite cleavages were polished using diamond powder, after which areas of 10 × 10 mm were mapped. The X-ray fluorescence spectra were acquired at three points at a long acquisition time.

The Mössbauer spectra were recorded using an MS1104Em spectrometer, operating in the constant acceleration mode with a triangular change in the Doppler velocity of the source relative to the absorber. The source was ^{57}Co in a Rh matrix. The experiments were performed at temperatures of 15–300 K in a CCS-850 closed-cycle helium cryostat (Janis Research). Model decoding and analysis of the Mössbauer spectra were implemented using SpectrRelax software [42]. The isomeric chemical shifts were determined relative to the metal α-Fe.

The IR spectra were obtained at room temperature in air using a Vertex70 Fourier spectrometer (Bruker). The measurements were carried out in the reflection mode using an attenuated total reflectance (ATR) device with a diamond crystal.

The Fe and Ni *K*-edge XAS spectra of the chondrites and reference samples (FeO and α-Fe_2O_3 oxides and metal Ni) were measured at the BM31 line of the European Synchrotron Radiation Facility (ESRF, Grenoble, France). The spectra were recorded in the transmission mode upon continuous scanning using a Si (111) double-crystal monochromator in the energy range of 6.5 to 8.5 keV, taking about 20 min per spectrum. In order to perform calibration, the spectrum of iron foil was measured simultaneously with spectrum acquisition of each sample by means of a third ionization chamber. Data processing (background subtraction and signal normalization) was performed using the Demeter Athena software [43].

RESULTS AND DISCUSSION

The first step was to study the elemental composition of the Markovka, Polujamki and Jiddat Al Harasis 055 chondrites via micro-XRF. All the samples revealed the presence of Fe, Mg, Al, Si, S, Ca, Ti, Cr, Mn, and Ni; the furthermore, Markovka chondrite included K, and the Polujamki chondrite contained also P and As elements. Since the meteorite samples are chemically inhomogeneous, the use of micro-XRF enabled us to obtain the distribution maps of chemical elements detected on the sample surface. The primary radiation

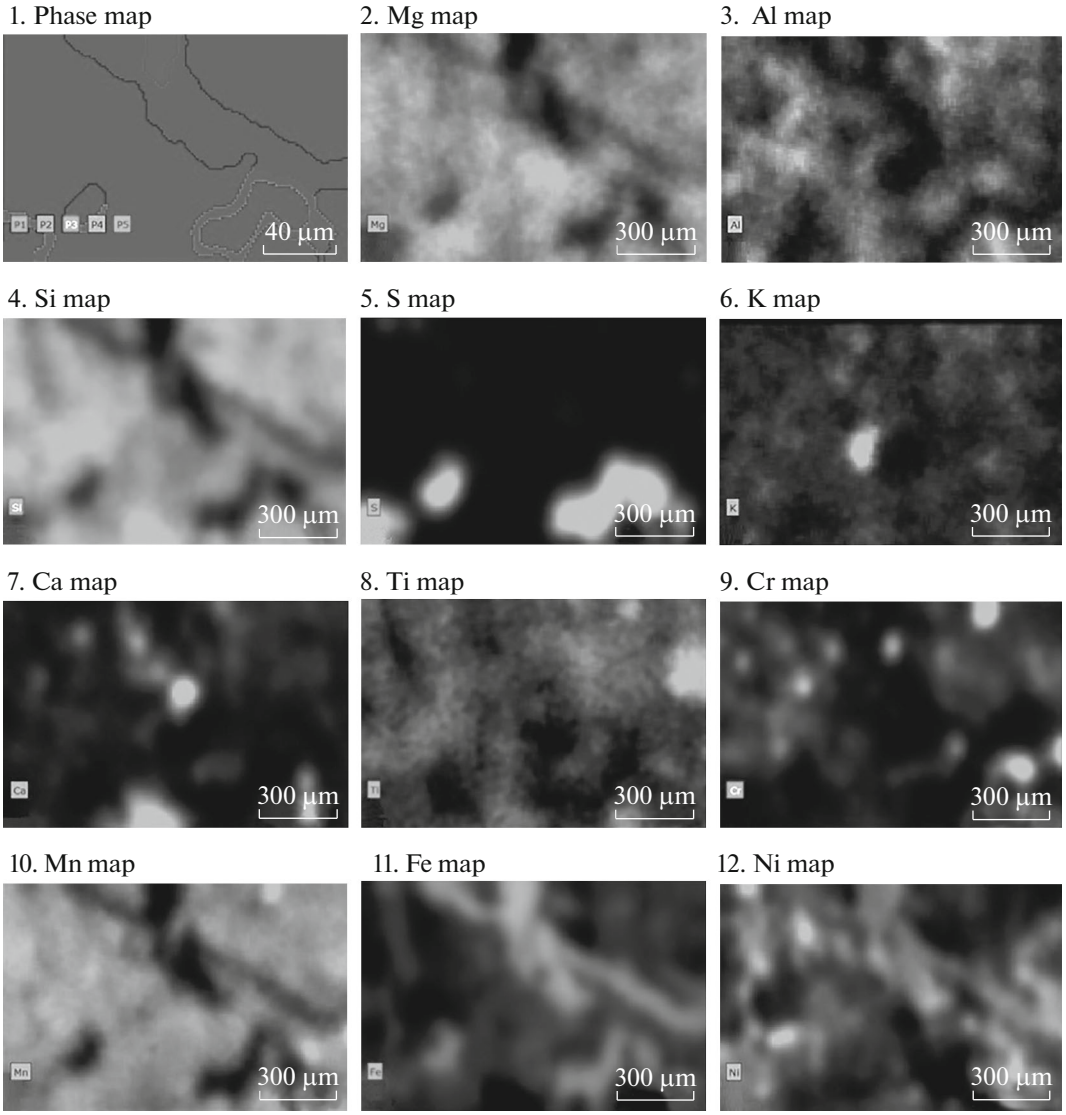

Fig. 1. Micro-XRF element mapping of the Markovka chondrite. Areas with different chemical-element contents (1), as well as the Mg, Al, Si, S, K, Ca, Ti, Cr, Mn, Fe, and Ni maps (2–12) are given.

in the M4 TORNADO microfluorescence spectrometer was focused using a polycapillary lens which focuses radiation from the X-ray tube into a spot with a diameter of 25 μm at a specific point on the sample surface. Identification and analysis of different components (P1, P2... phases) of the inhomogeneous samples were implemented via the standard mathematical toolbox of the spectrometer (the "Area" method) based on the fluorescence intensity measured at different points of the probed surface. In this method, points with an identical chemical composition merge into components. The areas of individual components depend on the selected sensitivity which is a parameter of the "Area" method.

Figure 1 displays the element mapping data for the Markovka chondrite; similar element distribution maps were also acquired for the other samples (Polujamki and Jiddat Al Harasis 055). The chemical-element concentrations were determined from the fundamental parameters using the standard mathematical toolbox of the spectrometer. Element mapping analysis reveals that the chondrites are composed of several components that define surface areas formed by chemical-element aggregates with similar concentrations. The chemical-element concentrations in different components observed via micro-XRF (P1, P2, P3, P4, and P5) in the Markovka chondrite are listed in Table 1.

A comparative distribution of Fe, Ni, Mg, Si, Ca, and Al elements within the micro-XRF maps for the three samples is given in Fig. 2. There are clearly distinguished surface areas with varying concentrations of the main chemical elements (Fe, Mg, Ni, and Si) composing the chondrites. Moreover, the Markovka

Table 1. Element content in components of the Markovka meteorite in accordance with micro-XRF data

Components	Fe	Mg	Si	Ni	S	Al	Ca	Mn	Cr	Ti	K
P1	35.49	23.29	33.41	2.21	0.91	1.53	1.78	0.54	0.60	0.11	0.12
P2	59.48	14.31	18.00	4.32	0.57	0.88	1.83	0.22	0.30	0.04	0.06
P3	50.91	10.88	13.35	2.99	19.63	0.85	0.78	0.17	0.32	0.04	0.08
P4	42.40	17.70	22.42	3.23	10.36	1.33	1.56	0.34	0.50	0.06	0.10
P5	82.79	2.66	6.87	5.93	0.25	0.54	0.76	0.01	0.12	0.02	0.05

and Jiddat Al Harasis 055 specimens contain areas with Ca and Al that are likely due to Ca- and Al-rich inclusions in the chondrite meteorites. Some components are also sulfur-enriched. Besides this, the Markovka chondrite includes areas with high concentrations of S, K, Cr, the Polujamki specimen reveals large amounts of Ca, S, P, Cr, and the Jiddat Al Harasis 055 chondrite is saturated with S and Cr.

The next step was to detect the iron-containing mineral phases in the Markovka, Polujamki and Jiddat Al Harasis 055 meteorites using Mössbauer spectra measured at different temperatures. Figure 3 shows the Mossbauer spectra of the Markovka chondrite, acquired at room temperature and at a temperature of 15 K. The parameters of the Mössbauer spectra are listed in Table 2. The Mossbauer spectra are composed of 3 doublets and 4 sextets. The isomeric shifts δ of doublets *D*1 and *D*2 are almost equal and correspond to Fe^{2+} ions [44]. The quadrupole splittings Δ of doublets *D*1 and *D*2 differ considerably and match the values Δ observed for doublets of Fe^{2+} ions in olivines and pyroxenes, respectively [45–48]. The doublet *D*3 possesses a value δ, corresponding to Fe^{3+} ions [44]. The value Δ and the broadened lines of the doublet *D*3 are characteristic of Fe^{3+} ions in iron oxides and hydroxides in the superparamagnetic state [49], which occurs when their crystallite sizes are less than 200 nm. If the particle size is rather small, then superparamagnetism causes the collapse of the Zeeman structure of the components in the Mössbauer spectrum into a doublet or a singlet [50]. A decrease in the temperature leads to a decrease in the effect of superparamagnetism on the structure of the Mössbauer spectrum [49]. When the temperature reaches 15 K, the value Δ of the doublet *D*3 decreases. Moreover, it reduces the doublet area and the sextet area *C*1 increases. The sextet *S*1 has a value of δ, corresponding to Fe^{3+} ions [44], as well as a low ultrafine magnetic-field value (*H*). A decrease in the temperature favors an increase in *H* for the sextet *S*1, whereas the line width is considerably reduced. The sextet *S*1 is likely due to Fe^{3+} ions in goethite particles [51, 52]. Since the area of the sextet *S*1 increases as the temperature decreases due to a decrease in the area of the doublet *D*3, both components are attributed to goethite particles with the average particle size distribution. The parameters of the sextet *S*2 are close to those observed for the Mössbauer spectrum of hematite nanoparticles [50]. The low room-temperature value *H* of the sextet *S*2 is due to the superparamagnetic effect. The value δ of the sextet *S*3 refers to Fe^{2+} ions, and the values of the quadrupole shift and ultrafine magnetic field tend to those of the Mössbauer spectra of troilite [45–48]. The sextet *S*4 has a value of δ typical for the metallic state. The parameters of the sextet S4 are almost equal to those of the sextet corresponding to kamacite [45–48]. The Mössbauer component areas are commensurate with the Fe^{3+}-ion concentrations in the appropriate phases. Hence, the Markovka sample contains the following iron-containing phases: olivine (19%), pyroxene (7%), goethite (52%), hematite (12%), troilite (7%), and kamacite (4%).

A similar analysis of the Mössbauer spectra was also implemented for the Polujamki and Jiddat Al Harasis 055 specimens. Table 3 shows the iron-containing phase contents for the Markovka, Polujamki and Jiddat Al Harasis 055 chondrites. It can be seen that all samples are predominantly composed of olivine and goethite with a small content of pyroxene and hematite. Besides this, the Markovka and Polujamki chondrites contain low amounts of troilite and kamacite.

The oxidation states of nickel and iron were afterwards estimated in the chondrites.

The oxidation state of iron is an important parameter in meteorite science because it depends on the physicochemical processes of meteorite formation (such as thermal metamorphism and hydration). Iron in recently formed meteorites may exist in the form of Fe^0 in a Fe—Ni metal, Fe^{2+} in silicates and sulfides and Fe^{3+} in phyllosilicates and magnetite. Over time, the oxidation of Fe^0 and Fe^{2+} iron forms transforms them into Fe^{3+}-enriched crystal phases [33, 53]. In the present work, the oxidation state of iron in the Markovka, Polujamki and Jiddat Al Harasis 055 chondrites was estimated by the combined analysis of Mössbauer and Fe *K*-edge XANES spectra. The oxidation state of nickel was determined using Ni *K*-edge XANES spectra.

According to Mössbauer spectroscopy data (Table 3), the average iron oxidation state in the Jiddat Al Harasis 055 chondrite is equal to +2.5 and those in the Markovka and Polujamki chondrites are +2.6.

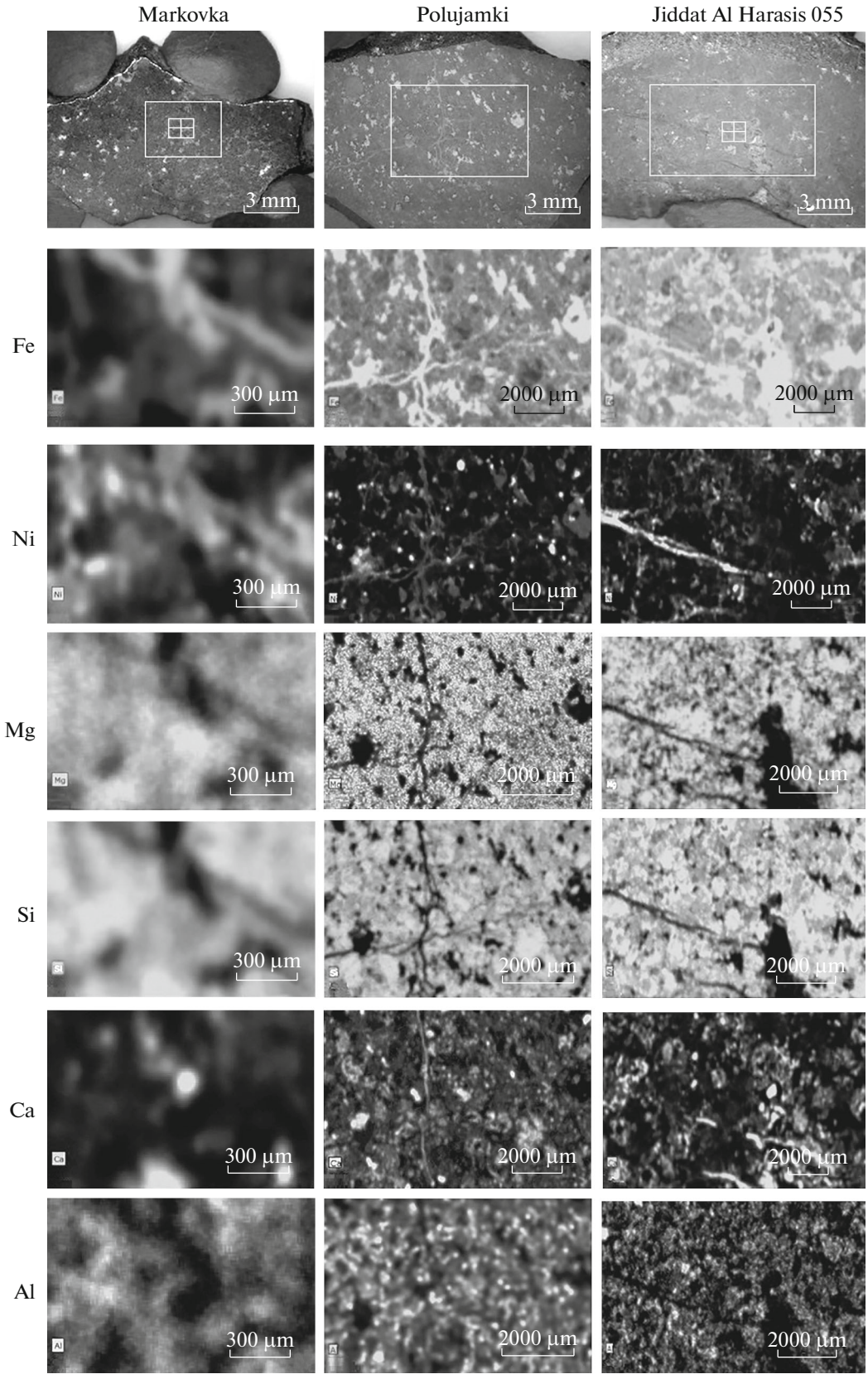

Fig. 2. Optical micrographs of the Markovka, Polujamki and Jiddat Al Harasis 055 chondrites (the upper series of images) along with the micro-XRF element distribution maps for Fe, Ni, Mg, Si, Ca, and Al in the Markovka, Polujamki and Jiddat Al Harasis 055 meteorites.

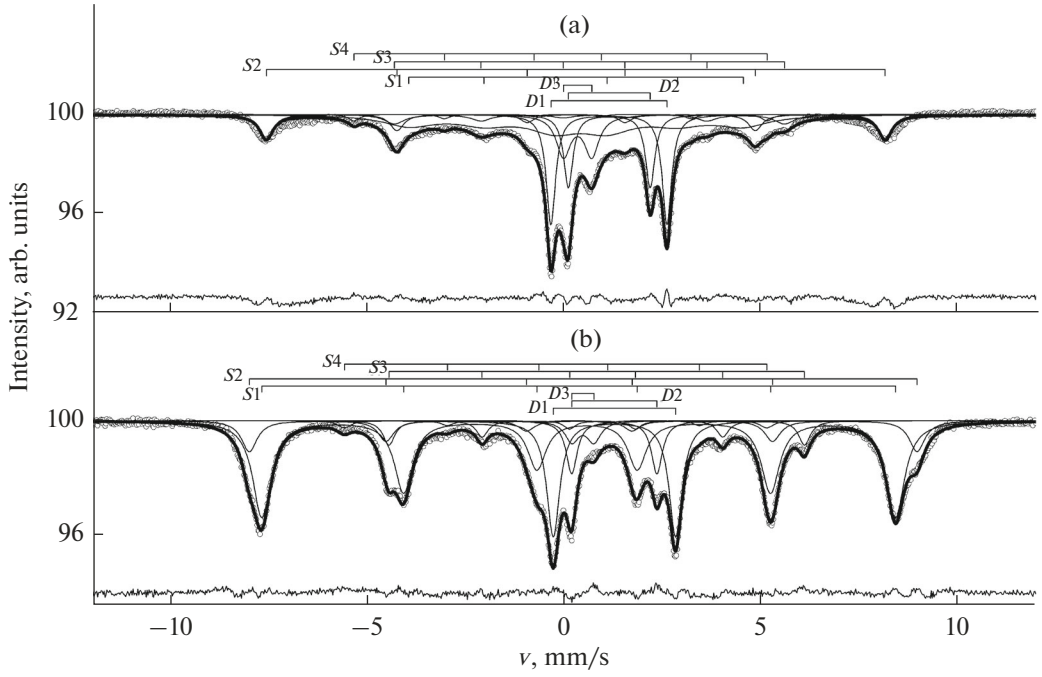

Fig. 3. Mössbauer spectra of the Markovka chondrite, acquired at (a) room temperature and (b) 15 K. The adjustment results for each spectrum are shown and the values extracted via fitting are listed in Table 2.

The Fe *K*-edge XANES spectra in the meteorites are given in Fig. 4. The oxidation state of iron was found on the basis of several XANES-based methods. First of all, the exact positions of the X-ray absorption edges of the chondrites (chemical shift) were analyzed. The interaction between X-ray radiation and the substance causes ionization of a deep core level. The XANES edge energies have strict values and are unique characteristics of materials. A variation in the oxidation state of an atom in a material leads to a change in the X-ray absorption edge energy due to a change in the effective charge at the atom, resulting in displacement of the core level energies. This effect can be used for evaluation of the unknown oxidation state

Table 2. Parameters of the Mössbauer spectra of the Markovka meteorite. δ—isomeric shift, ε—quadrupole displacement of Zeeman sextets, Δ—quadrupole splitting of paramagnetic components; *H*—ultrafine magnetic field at ^{57}Fe nuclei, *A*—component area, *G*—spectral line width, and χ^2—Pearson criterion

T, K	Component	δ ± 0.01, mm/s	ε/Δ ± 0.01, mm/s	*H* ± 1, kE	*A* ± 1, %	*G* ± 0.01, mm/s	Phase
300	D1	1.14	3.45		20	0.29	Olivine
	D2	1.15	2.08		13	0.29	Pyroxene
	D3	0.35	0.72		11	0.44	Goethite
	S1	0.37	−0.06	264	33	1.56	Goethite
	S2	0.36	−0.01	488	13	0.41	Hematite
	S3	0.71	−0.06	308	7	0.62	Troilite
	S4	0.00	−0.09	336	3	0.34	Kamacite
15	D1	1.28	3.10		19	0.40	Olivine
	D2	1.28	2.16		7	0.34	Pyroxene
	D3	0.48	0.56		4	0.42	Goethite
	S1	0.48	−0.11	500	48	0.56	Goethite
	S2	0.46	0.05	527	12	0.48	Hematite
	S3	0.91	−0.07	328	7	0.36	Troilite
	S4	0.01	−0.28	343	3	0.41	Kamacite

Table 3. Iron-containing phases of the Markovka, Polujamki and Jiddat Al Harasis 055 chondrites, determined via Mössbauer spectroscopy (relative iron concentrations)

Phase	Concentration, %		
	Jiddat Al Harasis 055	Markovka	Polujamki
Goethite (α-FeOOH)	35	49	42
Olivine	34	19	22
Hematite (α-Fe_2O_3)	18	12	15
Pyroxene	13	10	10
Troilite (FeS)	–	7	7
Kamacite (Fe–Ni alloy)	–	3	4

of atoms. Comparing the absorption-edge position in the sample with the unknown oxidation state of the chemical element of interest and that in the reference samples with known oxidation states of the atoms under investigation, one can find the sought oxidation state of the element. A recently described method was successfully applied for evaluation of the oxidation state of lanthanides in lanthanide-containing silicates [20, 21], which are promising from the viewpoint of the determination the natural conditions of mineral formation. In the present study, the Fe oxidation state was determined by comparing the Fe *K*-XANES spectra of the meteorites (with an unknown iron oxidation state) and reference samples (with a known iron oxidation state), FeO with an iron oxidation state of 2+, and α-$Fe_2^{3+}O_3$ with an iron oxidation state of 3+. The absorption-edge position was determined at points, where the normalized absorption coefficient takes values of 0.4 and 0.6 (these values are empirical and chosen for averaging).

Secondly, the oxidation states of iron were assessed via analysis of the pre-edge feature of the Fe *K*-XANES spectra based on the method described in work [53]. This method involves correlation of the intensity and centroid energy of the pre-edge feature of the Fe *K*-XANES spectrum. Comparing the positions in the dependence of the pre-edge intensity on the pre-edge energy for the samples (with unknown oxidation states and coordination numbers of Fe) and those for the reference samples (with known oxidation states and coordination numbers of Fe), one can estimate oxidation states and coordination numbers of iron in the investigated samples. This method was recently applied in the analysis of oxidation states of iron in a series of impact glasses from the Zhamanshin crater [54].

After that, the average oxidation states of iron were determined using the above methods. The average oxidation states of iron in the bulk of the Markovka, Polujamki and Jiddat Al Harasis 055 chondrites were found to be 2.4+, which is in agreement with the Mössbauer spectroscopy data. The slight variations in the oxidation states of iron, estimated via Mossbauer and XANES spectroscopies, seem to be due to the fact that the resolution of the MS1104Em Mossbauer spectrometer is too weak to distinguish Fe^{2+} ions in the M3 position of olivine and pyroxene.

Figure 5 displays the magnified pre-edge region of the Fe *K*-XANES. As seen, the intensity of the pre-edge feature of the Fe *K*-XANES spectrum of the Polujamki meteorite is higher than that of the pre-edge feature of the Markovka and Jiddat Al Harasis 055 meteorite samples, in spite of the fact that the pre-edge intensity of the Fe *K*-XANES spectrum depends on the iron coordination [55]. Hence the higher intensity of the pre-edge feature of the XANES spectrum of the Polujamki chondrite reflects a lower coordination number of iron and stronger distortion from the octahedral symmetry in this sample, as compared to Markovka and Jiddat Al Harasis 055.

The Ni *K*-edge XANES spectra of the Markovka, Polujamki and Jiddat Al Harasis 055 chondrites, as well as the spectra of the reference samples, such as Ni^0 metal nickel and $Ni^{2+}O$ nickel oxide, are given in

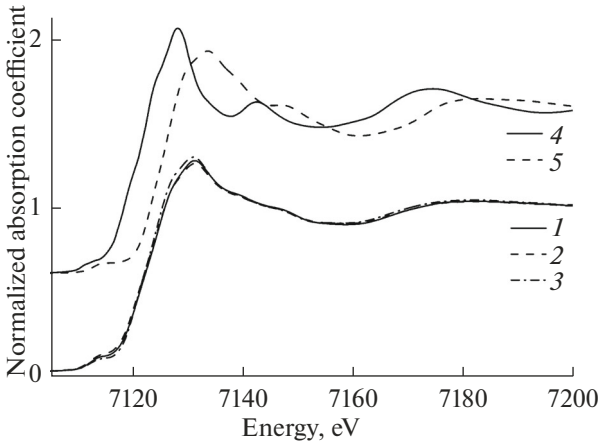

Fig. 4. Fe *K*-XANES spectra of Markovka (*1*), Polujamki (*2*) and Jiddat Al Harasis 055 (*3*) chondrites in comparison with the spectra of $Fe^{2+}O$ (*4*) and α-$Fe_2^{3+}O_3$ (*5*) reference samples.

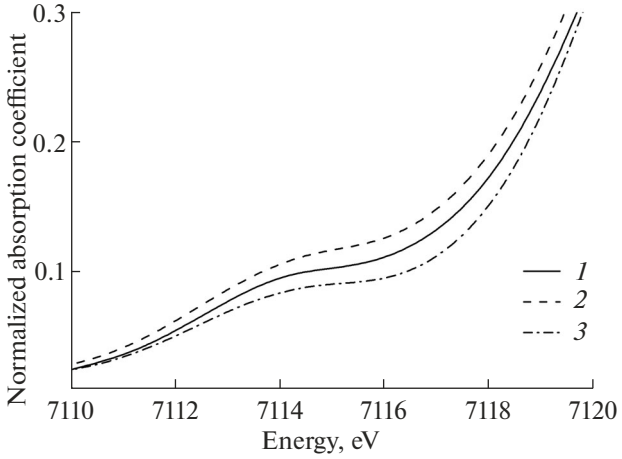

Fig. 5. Pre-edge feature of the Fe *K*-XANES spectra of the Markovka (*1*), Polujamki (*2*) and Jiddat Al Harasis 055 (*3*) chondrites.

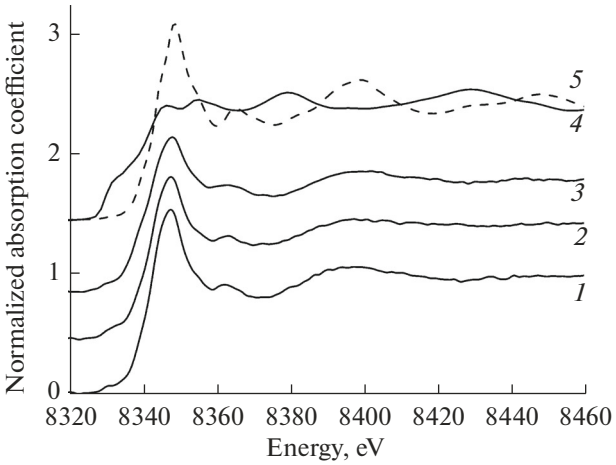

Fig. 6. Ni *K*-XANES spectra of the Markovka (*1*), Polujamki (*2*) and Jiddat Al Harasis 055 (*3*) chondrites and reference samples — metallic Ni (*4*) and NiO (*5*, dotted line).

Fig. 6. It is evident that the chondrites are depleted of metal Ni and most nickel atoms are in the Ni^{2+} state.

In addition to X-ray and Mössbauer spectroscopy data, the Markovka, Polujamki and Jiddat Al Harasis 055 samples were also probed via IR spectroscopy (Fig. 7). Shock deformations play a key role in many meteorites and allow one to recover their geological history. On the other hand, the IR spectra of meteorites are sensitive to shock-induced disordering [12]. In the case of shocked pyroxenes and olivines, there is well-known broadening and displacement of the peaks, due to chemical changes (refer to Table 3 in [12]). Moreover, the shock may cause the formation of complex mineral structures, mainly feldspars along with pyroxene. As follows from Fig. 7, the Markovka, Polujamki and Jiddat Al Harasis 055 chondrites underwent strong shock-induced deformation. The characteristic absorption band at 852–864 cm^{-1} was shifted by more than 13 cm^{-1}, whereas the band at 1055 cm^{-1} was displaced by 3 cm^{-1} relative to natural samples.

CONCLUSIONS

A complex study of the Markovka (H4 petrological type), Polujamki (H4 type) and Jiddat Al Harasis 055 (L4-5 type) chondrites was performed using X-ray and Mössbauer spectroscopy methods, as well as IR spectroscopy. The elemental composition of the chondrites was determined via micro-XRF, and element distribution maps were obtained. The Fe-containing phases of the meteorites were analyzed via Mössbauer spectroscopy. All meteorite samples were found to be composed of olivine and goethite with a small amount of pyroxene and hematite. Low troilite and kamacite contents were also observed in the Markovka and Polujamki samples. The oxidation states of Fe in the chondrites were assessed through the combined analysis of Mössbauer spectroscopy and Fe *K*-edge XANES data. According to the Mössbauer spectroscopy data, the average Fe oxidation state in the Markovka and Polujamki meteorites is +2.6 and that in the Jiddat Al Harasis 055 meteorite is +2.5. Analysis of the Fe *K*-edge XANES spectra revealed the average oxidation state of iron to be +2.4 in all samples, which was commensurate with the Mössbauer spectroscopy data. As established from the Ni *K*-edge XANES spectra, most Ni atoms in the meteorites have an oxidation state of 2+. Based on the IR spectroscopy data, the chondrites underwent strong shock-induced deformation. The results are expected to make a contribution to statistical information on the chemical composition and structure of ordinary chondrites, as well as being useful for the further estimation of processes that occur during the formation of a protoplanetary disk,

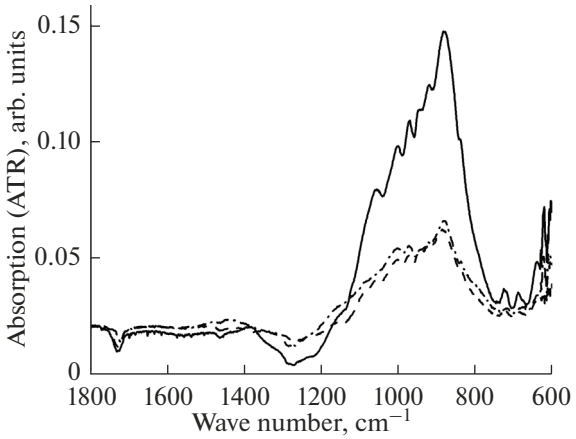

Fig. 7. IR spectra of Markovka (*1*), Polujamki (*2*) and Jiddat Al Harasis (*3*) meteorites, recorded in the reflection (ATR) mode.

including coagulation and differentiation of the interstellar substance in the early Solar System.

ACKNOWLEDGMENTS

We are grateful to A. A. Tereshchenko for help in acquiring the IR spectroscopy data.

FUNDING

This work was supported by the Ministry of Education and Science of the Russian Federation (state task no. 16.3871.2017/4.6).

REFERENCES

1. J. Aramendia, L. Gomez-Nubla, K. Castro, et al., Trends Anal. Chem. **98,** 36 (2018). https://doi.org/10.1016/j.trac.2017.10.018
2. K. C. Daviau, R. G. Mayne, and A. J. Ehlmann, *43rd Lunar Planet. Sci. Conf* (The Woodlands, TX, 2012).
3. I. Torre-Fidez, J. Aramendia, L. Gomez-Nubla, et al., Anal. Bioanal. Chem **410,** 7477 (2018). https://doi.org/10.1007/s00216-018-1363-5
4. M. Haschke, U. Rossek, R. Tagle, and U. Waldschläger, Adv X-Ray Anal. **55,** 286 (2012).
5. J. M. Cadogan, L. Rebbouh, J. V. J. Mills, and P. A. Bland, Hyperfine Interact. **222** (Suppl. 2), 91 (2013). https://doi.org/10.1007/s10751-012-0644-1
6. A. A. Maksimova, M. I. Oshtrakh, E. V. Petrova, et al., Hyperfine Interact. **237,** 134 (2016). https://doi.org/10.1007/s10751-016-1344-z
7. N. N. Elewa and J. M. Cadogan, Hyperfine Interact. **238,** 4 (2017). https://doi.org/10.1007/s10751-016-1350-1
8. N. N. Elewa, R. Cobas, and J. M. Cadogan, Hyperfine Interact. **237,** 107 (2016). https://doi.org/10.1007/s10751-016-1315-4
9. W. Sato, M.·Nakagawa, N. Shirai, and M. Ebihara, Hyperfine Interact. **239,** 13 (2018). https://doi.org/10.1007/s10751-018-1489-z
10. Y. Kebukawa, C. M. O'D. Alexander, and G. D. Cody, Geochim. Cosmochim. Acta **75,** 3530 (2011). https://doi.org/10.1016/j.gca.2011.03.037
11. C. M. O'D. Alexander, G. D. Cody, Y. Kebukawa, et al., Meteorit. Planet. Sci **49** (4), 503 (2014). https://doi.org/10.1111/maps.12282
12. A. Kereszturi, I. Gyollai, Zc. Kereszty, et al., Spectrochim. Acta A Mol. Biomol. Spectrosc. **173,** 637 (2017). https://doi.org/10.1016/j.saa.2016.10.012
13. I. Gyollai, A. Kereszturi, Z. Kereszty, et al., Centr. Eur. Geol. **60/2,** 173 (2017). https://doi.org/10.1556/24.60.2017.007
14. Y. A. Abdu, F. C. Hawthorne, and M. E. Varela, Astrophys. J. Lett. **856,** L9 (2018). https://doi.org/10.3847/2041-8213/aab433
15. G. Bunker, *Introduction to XAFS: A Practical Guide to X-Ray Absorption Fine Structure Spectroscopy* (Cambridge University Press, Cambridge, 2011).
16. *X-Ray Absorption and X-Ray Emission Spectroscopy. Theory and Applications,* Ed. by J. van Bokhoven and C. Lamberti, (Wiley, Chichester, UK, 2016).
17. A. N. Kravtsova, L. V. Guda, O. E. Polozhentsev et al., J. Struct. Chem. **59** (7), 1691 (2018). https://doi.org/10.26902/JSC20180725
18. A. J. Berry, P. F. Schofield, A. N. Kravtsova, et al., Chem. Geol. **466,** 32 (2017). https://doi.org/10.1016/j.chemgeo.2017.03.031
19. A. N. Kravtsova, A. V. Soldatov, A. M. Walker, and A. J. Berry, J. Phys. Conf. Ser. **712,** 012089 (2016). https://doi.org/10.1088/1742-6596/712/1/012089
20. A. N. Kravtsova, A. A. Guda, J. Goettlicher, et al., J. Phys. Conf. Ser. **712,** 012096 (2016). https://doi.org/10.1088/1742-6596/712/1/012096
21. A. N. Kravtsova, A. A. Guda, A. V. Soldatov, et al., Opt. Spectrosc. **119** (6), 982 (2015). https://doi.org/10.7868/S003040341511015X
22. I. S. Rodina, A. N. Kravtsova, A. V. Soldatov, et al., Opt. Spectrosc. **115** (6), 858 (2013). https://doi.org/10.7868/S0030403413120179
23. I. S. Rodina, A. N. Kravtsova, A. V. Soldatov, and A. J. Berry, Opt. Spectrosc. **111** (6), 936 (2011).
24. I. S. Rodina, A. N. Kravtsova, M. A. Soldatov, et al., J. Phys. Conf. Ser **190,** 012181 (2009). https://doi.org/10.1088/1742-6596/190/1/012181
25. Y. Kebukawa, M. E. Zolensky, A. L. D. Kilcoyne, et al., Meteorit. Planet. Sci **49,** 2095 (2014).
26. Y. Kebukawa, M. E. Zolensky, M. Fries, et al., *47th Lunar Planet. Sci. Conf.* (The Woodlands, TX, 2016), p. 1802.
27. S. Wirick, G. J. Flynn, C. Jacobsen, and L. P. Keller, *37th Lunar Planet. Sci. Conf.* (The Woodlands, TX, 2006).
28. H. Yabuta, S. Amari, J. Matsuda, et al., *41st Lunar Planet. Sci. Conf.* (The Woodlands, TX, 2010), p. 1202.
29. F. L. le Formal, N. Guijarro, W. S. Bourée, et al., Energy Environ. Sci **9,** 3448 (2016). https://doi.org/10.1039/C6EE02375D
30. M. Bose, R. A. Root, and S. Pizzarello, Meteorit. Planet. Sci **52,** 546 (2017). https://doi.org/10.1111/maps.12811
31. H. Ono, A. Takenouchi and T. Mikouchi, *79th Annual Meeting of the Meteoritical Society* (Berlin, Germany, 2016).
32. A. J. King, P. F. Schofield, J. F. W. Mosselmans, and S. S. Russell, *77th Annual Meeting of the Meteoritical Society* (Casablanca, Morocco, 2014).
33. A. Garenne, P. Beck, G. Montes-Hernandez, et al., *45th Lunar Planet. Sci. Conf.* (The Woodlands, TX, 2014).
34. F. -R. Orthous-Daunay, E. Quirico, L. Lemelle, et al., Earth Planet. Sci. Lett. **300,** 321 (2010). https://doi.org/10.1016/j.epsl.2010.10.012
35. P. Beck, V. De Andrade, F. -R. Orthous-Daunay, et al., Geochim. Cosmochim. Acta **99,** 305 (2012). https://doi.org/10.1016/j.gca.2012.04.041
36. A. Ali, S. J. Nasir, I. Jabeen, et al., Meteorit. Planet. Sci **52,** 1991 (2017). https://doi.org/10.1111/maps.12903

37. T. Yokoyama, K. Misawa, O. Okano, et al., Earth Planet. Sci. Lett. **458,** 233 (2017). https://doi.org/10.1016/j.epsl.2016.10.037
38. S. Wirick, G. J. Flynn, S. Sutton, and M. E. Zolensky, *45th Lunar Planet. Sci. Conf.* (The Woodlands, TX, 2014).
39. A. N. Mikhanov and N. D. Kotel'nikova, Meteoritika **47,** 20 (1988).
40. O. A. Kirova, M. I. D'yakonova, and V. Ya Kharitonova, Meteoritika **34,** 57 (1975).
41. S. S. Russell, L. Folco, M. M. Grady, et al., Meteorit. Planet. Sci **39,** A 215 (2004).
42. M. E. Matsnev and V. S. Rusakov, AIP Conf. Proc **1489,** 178 (2012). https://doi.org/10.1063/1.4759488
43. B. Ravel and M. Newville, J. Synchrotron Radiat **12,** 537 (2005). https://doi.org/10.1107/S0909049505012719
44. F. Menil, J. Phys. Chem. Solids **46** (7), 763 (1985). https://doi.org/10.1016/0022-3697(85)90001-0
45. Y. A. Abdu and T. Ericsson, Meteorit. Planet. Sci **32,** 373 (1997).
46. E. Dos Santos, J. Gattacceca, P. Rochette, et al., Phys. Earth Planet. Inter. **242,** 50 (2015). https://doi.org/10.1016/j.pepi.2015.01.004
47. B. S. Paliwal, R. P. Tripathi, H. C. Verma, et al., Meteorit. Planet. Sci **35,** 639 (2000).
48. A. M. Gismelseed, Y. A. Abdu, M. H. Shaddad, et al., Meteorit. Planet. Sci **49,** 1485 (2014).
49. S. Bedanta and W. Kleemann, J. Phys. D: Appl. Phys. **42,** 013001 (2009).
50. W. Kündig and H. Bömmel, Phys. Rev. **142,** 327 (1966). https://doi.org/10.1103/PhysRev.142.327
51. S. Bocquet, R. J. Pollard, and J. D. Cashion, Phys. Rev. **46,** 11657 (1992). https://doi.org/10.1103/PhysRevB.46.11657
52. U. Schwertmann, P. Cambier, and E. Murad, Clays Clay Miner. **33,** 369 (1985).
53. M. Wilke, F. Farges, P. -E. Petit, et al., Am. Mineral. **86,** 714 (2001). https://doi.org/10.2138/am-2001-5-612
54. A. N. Kravtsova, L. V. Guda, A. A. Guda, et al., Radiat. Phys. Chem. (in press). https://doi.org/10.1016/j.radphyschem.2018.12.017
55. G. Giuli, S. G. Eeckhout, E. Paris, et al., Meteorit. Planet. Sci. **40**, 1575 (2005). https://doi.org/10.1111/j.1945-5100.2005.tb00132.x

Translated by O. Maslova